Chapter 15
Compartmental Population Balances by Means of Monte Carlo Methods

Gregor Kotalczyk and Frank Einar Kruis

Abstract Stochastic simulation techniques for the solution of a network of population balance equations (PBE) are discussed in this chapter. The application of weighted Monte Carlo (MC) particles for the solution of compartmental PBE systems is summarized and its computational efficacy in form of a parallel GPU implementation is pointed out. Solution strategies for coagulation, nucleation, breakage, growth and evaporation are thereby presented. An application example treats the simultaneous coagulation, nucleation, evaporation and growth encountered during particle production through the aerosol route. Furthermore, the simulation of a compartmental network is discussed and parallel simulation techniques for the transport of weighted MC particles are presented. The proposed methodology is benchmarked by comparison with a pivot method for a variety of test cases with an increasing degree of complexity. Simulation conditions are identified, for which conventional, non-weighted MC simulation techniques are not applicable. It is found, that the specific combination of a screen unit with tear-streams cannot be simulated by conventional methods, termed 'random removal', and make thus other techniques—like the here introduced merging techniques necessary.

Nomenclature

b	Breakage rate [s^{-1}]
d_g	Geometric mean diameter [m]
C_{dist}	Compare distance on GPU memory (integer) [–]
d^*	Kelvin diameter [m]
d	Diameter of particle [m]
$E_{i,j}$	Merging error of particles i and j [–]

G. Kotalczyk · F. E. Kruis (✉)
Institute of Technology for Nanostructures (NST),
University of Duisburg-Essen, Duisburg, Germany
e-mail: einar.kruis@uni-due.de

G. Kotalczyk
e-mail: gregor.kotalczyk@uni-due.de

S. Heinrich (ed.), *Dynamic Flowsheet Simulation of Solids Processes*,
https://doi.org/10.1007/978-3-030-45168-4_15

$f_{A\to B}$	Relative particle exchange flow rate from compartment A to B [s^{-1}]
$F_{A\to B}$	Absolute particle exchange flow rate from compartment A to B [s^{-1}]
G	Growth rate [m s^{-1}]
k_B	Boltzmann constant [J K^{-1}]
m_1	Atomic (resp, molecule) mass [kg]
N_MC	Number of MC simulation particles [–]
N_G	Concentration of gas atoms (or molecules) [m^{-3}]
$n_C(v)$	PSD in compartment C [m^{-6}]
o_idx	Destination index on GPU memory (integer) [–]
i^*	Number of atoms (resp. molecules) in critical cluster [–]
$p_A^{(i)}$	i-th property of particle A [unit of i-th property]
p_s	Saturation pressure [Pa]
$Q_{A\to B}$	Volumetric flow rate of carrier gas/liquid from compartment A to B [m^3 s^{-1}]
R	Mixing ratio for breakage scheme [–]
R_N	Nucleation rate [m^{-3} s^{-1}]
S	Supersaturation [–]
S_sep	Separation function for screen [–]
s_f	Reciprocal of stochastic resolution [m^{-3}]
T	Temperature [K]
t	(simulation) time [s]
t_char	Characteristic time [s]
v	Particle volume [m^3]
v^*	Kelvin volume [m^3]
v_M	Atomic (resp. molecular) volume [m^3]
V_C	Volume within compartment C filled with carrier liquid (or gas) [m^3]
W_i	Statistical weight of MC particle i [m^{-3}]
α_i	Merging weight for property i
β	Coagulation kernel [m^3 s^{-1}]
γ	Breakage function [–]
ε	Maximal admittable merging error [–]
τ	Time step [s]
σ	Surface tension [N m^{-2}]

Indices

0	Initial values

1 Introduction

The solution of the population balance equation (PBE) [1] plays an important role in a wide area of applications ranging from natural sciences to many fields of engineering [2]. Especially the modelling of chemical engineering problems such as crystallization [3], milling [4], granulation [5] or particle production in aerosol reactors [6] resort to PBE based process modelling.

The modelling of single apparatuses can be seldomly done with the assumption of spatial uniformity (as in e.g. [7]) and the application of Computational Fluid Dynamics (CFD) simulations and/or compartmental modelling becomes necessary in order to describe different zones of single apparatuses correctly.

CFD modelling allows a very high spatial resolution of the investigated system: 30,000 [8]−1,000,000 [9] cells are sometimes applied. The drawback of a CFD-PBE modelling is its enormous computational cost, hence a PBE has to be solved for each of these cells. Due to the high computational cost, only a rough approximation of the particle size distribution (PSD) is encountered in such simulations which typically resort to sectional methods with a low resolution (of ca. 12–30 discrete points or sections [10, 11]) or to the method of moments [12, 13], limiting the particle modelling mostly to one property—the size.

To overcome this problem, compartmental modelling is often applied, simplifying the spatial complexity to a low number of compartments (examples are 3 compartments or 10 compartments [14]). This allows, on the other hand, a more complex particle modelling with a more detailed sectional grid (e.g. 1000 discrete sections for 3 compartments [15]) or even with a Monte Carlo (MC) simulation, where more than one particle property allow to model a more complex morphology of the particles [14].

The PBE for a network of compartments, like presented in Fig. 1. can be described by the following formula:

$$
\begin{aligned}
\frac{\mathrm{d}n_C(v,t)}{\mathrm{d}t} = &+ \underbrace{\frac{1}{2}\int_0^v \beta_C(v', v-v')n_C(v',t)n_C(v-v',t)\mathrm{d}v'}_{\text{coagulation birth term}} \\
&- \underbrace{n_C(v,t)\int_0^\infty \beta_C(v,v')n_C(v',t)\mathrm{d}v'}_{\text{coagulation death term}} \\
&+ \underbrace{R_{\mathrm{N},C}(t)\cdot\delta(v-v_C^*(t))}_{\text{nucleation}} \underbrace{-\nabla_v(G_C(v,t)n_C(v,t))}_{\text{growth(G>0)/evaporation(G<0)}} \\
&\underbrace{-b_C(v)\cdot n_C(v,t)}_{\text{breakage death term}} + \underbrace{\int_v^\infty b_C(v')\cdot n_C(v',t)\cdot\gamma_C(v|v')\mathrm{d}v}_{\text{breakage birth term}} \\
&+ \sum_{\text{inflow from all compartments } i} f_{i\to C}\cdot n_i(v,t) \\
&- \sum_{\text{outflow to all compartments } i} f_{C\to i}\cdot n_C(v,t)
\end{aligned}
\tag{1}
$$

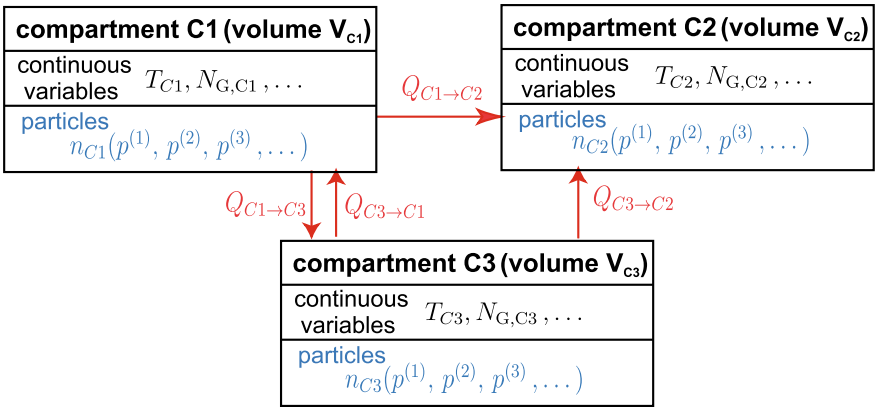

Fig. 1 A network of compartments. Each compartment C_i models parts of a reactor (or equipment) volume, which is filled with the carrier gas (or liquid) with a volume V_C. The compartment contains a PSD, n_C, and is described by other continuous variables, like temperature T_C, a gas concentration $N_{\mathrm{G},C}$, etc

where the coagulation kernels β_C, growth rates G_C, nucleation rates $R_{\mathrm{N},C}$ and sizes of the nucleating particles v_C^*, breakage rates $b_C(v)$ and breakage functions $\gamma_C(v|v')$ can be defined differently for each compartment C . The shown particle exchange flowrates $f_{i\to C}$ and $f_{C\to i}$ may assume constant values, or reflect more complex—nonlinear—and particle size or time dependent forms. The given volumetric flow rates $Q_{A\to B}$ (shown in Fig. 1) of the carrier gas (or liquid) and the volumes of the carrier gas (or liquid) of the outflow compartments, V_A, are thereby used in order to determine the particle exchange flowrates via:

$$f_{A\to B} = Q_{A\to B}/V_A \tag{2}$$

In this way, a complex reactor structure can be modelled in more detail [16, 17] or the interconnection of single processing units in a flowsheet simulation can be analyzed [15, 18, 19].

Although Eq. (1) describes only one particle property, the volume v, one could interpret v as a vector describing multiple properties of the particle, such as volume ($p^{(1)}$), surface area ($p^{(2)}$), wet content ($p^{(3)}$), and so on, as suggested in Fig. 1. Only a stochastic modelling is able to solve Eq. (1) for a high number of properties and render the complete particle morphology.

In the following, stochastic solution strategies for Eq. (1) will be discussed in the frame-work of an operator splitting approach meaning that the single processes coagulation, nucleation, growth/evaporation, breakage and transport of particles are decoupled for short periods of time τ. The approximation error introduced by this decoupling can be minimized by a choice of a low enough separation time step τ. For this reason, the solution strategies for single processes, like coagulation, nucleation, growth/evaporation and breakage are discussed for one compartment first. The

implementation of the coagulation in the framework of a compartmental network, as well as the transport between single compartments is discussed in the section afterwards, where the modelling of multiple compartments is applied.

2 Weighted Monte Carlo Particles for the Solution of the Population Balance Equation

The use of weighted simulation particles (a particle with weight w represents w real particles within a given reactor volume) has several advantages: it allows to describe the interaction between simulation particles having different concentrations coming from different cells or compartments [14, 20, 21]. It can also be used as a tool to control the number of simulation particles (e.g. to gain numerical accuracy). In the following, some techniques will be introduced to solve the single mechanisms presented in Eq. (1) by the application of weighted MC particles.

2.1 Coagulation

The correct description of the coagulation rates for the weighted particles, especially for a complex coagulation scheme, like the one introduced Zhao et al. [22] shown in Fig. 2, poses a great difficulty.

The authors [22] presented the 'ficticious particle theory' which leads to the following modified coagulation kernel:

$$\beta^{(fp)} = \frac{2W_j \max\left(W_i, W_j\right)}{W_i + W_j}\beta \tag{3}$$

The weights of the particles are denoted by W_i and W_j. The coagulation kernel β describes the coagulation of the original (non-weighted) system—which might be the Brownian kernel for the free molecular regime, etc. The resulting coagulation rate is asymmetric, making a distinction necessary, whether particle i coagulates with j or vice versa. This definition is 1) difficult to understand conceptually and 2) difficult to extend on other process—like nucleation or transport of fictitious particles.

We developed in [23] the concept of the stochastic resolution which describes each coagulation in the frame-work of equally weighted MC-particles, where each MC-particle describes s_f real particles. The value for the parameter s_f can be set arbitrarily. Figure 2 shows that the setting $s_f = W_{\min} = \min\left(\mathrm{W_i}, \mathrm{W_j}\right)$ leads to the correct description of the coagulation-scheme. The scaling factor s_f depends on the chosen coagulation pair, so that different coagulation-events are described in different stochastic resolutions.

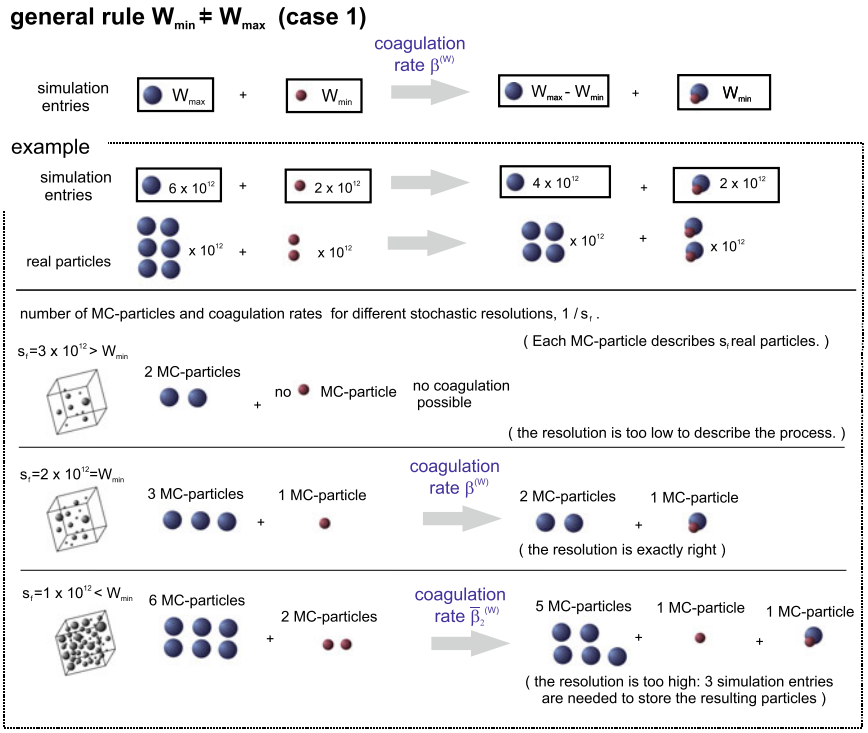

Fig. 2 The concept of 'stochastic resolution' can be used to describe the coagulation-scheme developed Zhao et al. [22]. Only the choice for $\mathbf{s_f} = \mathbf{W_{min}}$ leads to the correct description of the general rule presented in the 'simulation entries' line

The coagulation rate $\beta^{(w)}$ for this coagulation-scheme can be derived from the population balance equation:

$$\frac{\mathrm{d}n(v)}{\mathrm{d}t} = \frac{1}{2}\int_0^v \beta\left(v-v', v'\right)n\left(v-v'\right)n\left(v'\right)\mathrm{d}v' - n(v)\int_0^\infty \beta\left(v, v'\right)n\left(v'\right)\mathrm{d}v' \tag{4}$$

Instead of the 'original' concentrations $n(v)$, the concentrations of the MC-systems $n^{(MC)}(v) = \frac{n(v)}{s_f}$ are being considered. The multiplication of the PBE with the factor $\frac{1}{s_f} = \frac{1}{W_{\min}}$ leads to the following modified coagulation rate of the MC-particles: $\beta^{(MC)} = W_{\min} \cdot \beta$. Hence there is one MC-particle of the $W_{\min}$-species and $\frac{W_{\max}}{W_{\min}}$ MC-particles of the $W_{\max}$-species, the overall rate for the coagulation between one $W_{\min}$-MC-particle and one of the $W_{\max}$-MC-particles is:

$$\beta^{(w)} = \frac{W_{\max}}{W_{\min}} \cdot \beta^{(MC)} = W_{\max} \cdot \beta \tag{5}$$

The second case $W_{max} = W_{min}$, which is not shown in Fig. 2, is also described with the resolution $s_f = W_{min}$. Both particle species are described by only one MC-particle, so that only one MC-particle can be found after the coagulation. In order to apply the constant number scheme, the weight of the simulation entry representing this particle is divided by two and the particle properties are stored in both positions.

The thus derived coagulation kernel $\beta^{(w)}$ is easier to calculate than the originally introduced $\beta^{(fp)}$ —a speed up of the simulation up to 10% could be noticed. Due to its symmetric form, computational advantages for the implementation of the inverse method can be expected, as only half of the computations of the $\beta^{(w)}$ kernel are necessary. The simulation results of particle coagulation for the newly estimated coagulation kernel $\beta^{(w)}$ could be found to be as accurate as the $\beta^{(fp)}$-kernel results (which show excellent agreement with the solution produced by means of the Discrete-sectional-method in the first place) within the MC-stochastic noise [23].

2.2 Nucleation

Homogeneous nucleation is a mechanism that leads to the formation of new particles, which have to be included among the simulation entries. Constant number simulation-schemes sum up all possible algorithms, which update—somehow—the simulation properties, but keep the number of the used simulation entries constant. Keeping the number of simulation entries constant ensures a constant level of stochastic accuracy and makes a simple prediction of needed computational resources possible. Figure 3 shows possible constant-number nucleation algorithms. They can be used to model the inclusion of the nucleation particles or particles included by other processes: like breakage or transport.

The random removal algorithm has been introduced Lin et al. [24] in the framework of the concept of a 'constant number Monte Carlo simulation' which is based on the not-weighted particle scheme. The algorithms applying the merging step are based on the weighted-particles scheme and the concept of the merging error. They cannot be used for non-weighted MC simulations. The merge-List is created each 100 merge-steps and contains 100 simulation entries with low-weights.

2.2.1 Merging

The concept of 'merging' of simulation entries is proposed in [23]: if two simulation entries with exactly the same properties are merged, the resulting representation of the particle size distribution will not change and all the physical processes will be described in the same way. If the simulation entries differ slightly in their properties, a small error will be introduced.

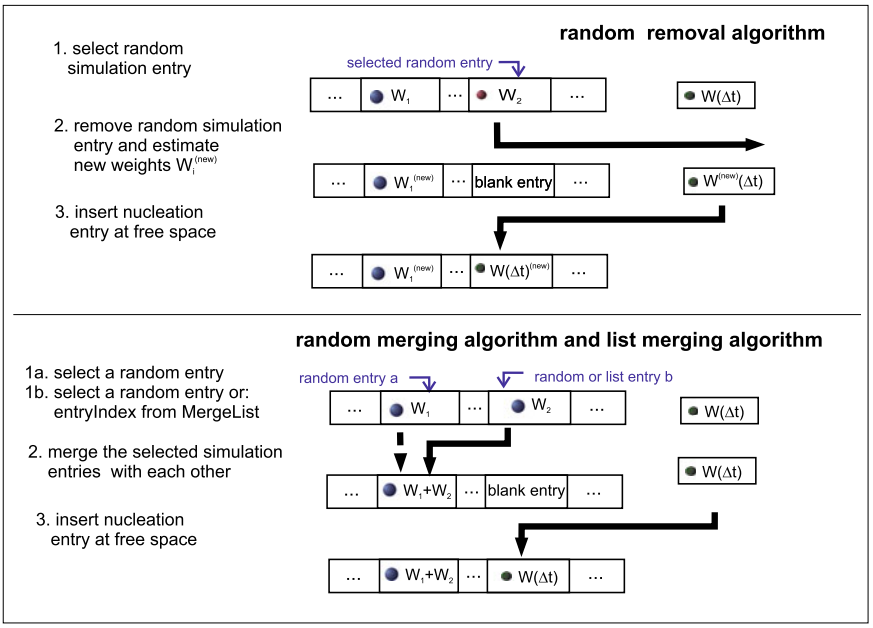

Fig. 3 Different simulation algorithms which combine the MC constant-number simulations based on weighted particles with the nucleation process

The merging scheme:
Each simulation entry contains the weight W, and other properties $p^{(1)}, p^{(2)}, p^{(3)}, \ldots$ of the rendered part of the particle population (where $p^{(i)}$ could be the volume, porosity, electric charge, etc.). If the simulation entry A (weight W_A) and B (weight W_B) are merged into the new simulation entry C (weight W_C and several properties $p_C^{(i)}$), the following two rules should apply:

(i) The total weight of the simulation-entries before and after the merge-step should be preserved:

$$W_C = W_A + W_B \tag{6}$$

(ii) If the total amount of the particle-properties is preserved one can write:

$$W_C \cdot p_C^{(i)} = W_A \cdot p_A^{(i)} + W_B \cdot p_B^{(i)} \Leftrightarrow p_C^{(i)} = \frac{W_A \cdot p_A^{(i)} + W_B \cdot p_B^{(i)}}{W_A + W_B} \tag{7}$$

This is the most simple assumption which should hold true for most of the physical applications, but other definitions—which make a more complex calculation necessary can be used. E.g., if the described property is the diameter d but the volume v is preserved, one can write (assuming sphere-like particles):

$$W_C \cdot \frac{\pi}{6}(d_C)^3 = W_A \cdot \frac{\pi}{6}(d_A)^3 + W_B \cdot \frac{\pi}{6}(d_B)^3$$
$$\Leftrightarrow d_C = \left(\frac{W_A \cdot (d_A)^3 + W_B \cdot (d_B)^3}{W_A + W_B}\right)^{1/3} \tag{8}$$

The merging error:
The error introduced into the simulation by the merging of the simulation entries can be estimated by the following formula:

$$E_{(A,B)} = \sum_{\text{all roperties } i} \alpha_i \cdot \left(\frac{p_A^{(i)} - p_B^{(i)}}{\min\left(p_A^{(i)}, \cdot p_B^{(i)}\right)}\right)^2 \tag{9}$$

where α_i are merging-weights, which can be set arbitrarily—depending on the physical process—they can be interpreted as a measure of the severity, which the deviation of the property $p_A^{(i)}$ from $p_B^{(i)}$ would have—compared to the deviation of other properties $p_A^{(j)}$ from $p_B^{(j)}$.

2.2.2 Parallel Merging Algorithm

The merging-algorithms presented in Fig. 3. use the selection of random simulation entries, resulting therefore in a random merging error $E_{(A,B)}$—which may be excessively high. The smallest possible merging error can be estimated by the comparison of all simulation-entry-pairs—which would prove very costly: $N_{\text{MC}} \cdot (N_{\text{MC}} - 1)/2$ comparisons are necessary, if N_{MC} simulation-entries are used. A sound compromise between both scenarios is the sampling of a 'representation of the simulation entries' and the estimation of the minimum merging error of this representation. A parallel algorithm can be applied for this purpose, easily adaptable for GPU computing: the merging errors for $(N_{\text{MC}} - 1)$ pairs of simulation-entries can be computed in parallel and the comparison of the calculated merging errors is done within only $\log_2 N$ computational steps, like shown in Fig. 4.

2.2.3 Validation of Coupled Coagulation and Nucleation

The nucleation is combined with the simulation of coagulation in two steps: First, a classical event-driven MC coagulation step is performed, this includes the selection of the coagulation pair via the fast parallel A/R-method introduced Wei [25] with the

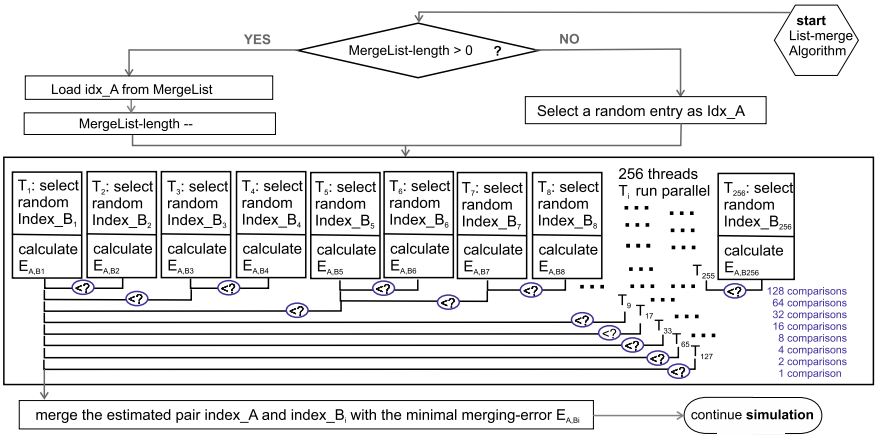

Fig. 4 The parallel low weight merging algorithm [23]: only 8 parallel thread-executions are necessary in order to estimate the pair (1 out of 256) of simulation-entries with the minimal merging error

weighting scheme based on the stochastic resolution—the actual time-step $\Delta\tau_{MC}$ is evaluated in this step, too. In a second step, the number of the nucleating particles is estimated, for this purpose the solution of the differential equation (which describes the nucleation) can be approximated by the Euler-method (more complicated Runge-Kutta methods or other ODE-solvers can be used for the modeling of the interaction with the continuous phase [26, 27]). The newly created simulation entry is then included by means of the merging algorithms from Fig. 4.

A typical benchmark test case[1] shows the advantage of the merging of particles compared to the random removal method, as sketched in Fig. 3. A part of the simulation results already discussed in [23] are summarized in Table 1, where the mean values d_g and standard deviations Δd_g of the geometric mean diameter are shown. Hence each MC simulation is executed with a different sequence of random numbers, the resulting geometric mean diameter $d_g^{(i)}$ is different for each simulation i. The arithmetic mean values (d_g) and standard deviations Δd_g of 100 $d_g^{(i)}$ values resulting from of 100 MC simulations are shown. (Similar findings could also be presented for the number concentration of the particles or the geometric standard deviations of the resulting PSDs.) It can be clearly seen that the application of merging techniques leads to significantly lower noise levels. For example, 10,000 simulation particles in combination with the random removal method cannot reach the same precision levels as the application of 1000 simulation particles in combination with the low

[1] A constant nucleation rate R_N is assumed, so that newly introduced simulation entries have the weight $W_0 = R_N \cdot \Delta\tau_{MC}$ and a predefined diameter d_0. For the simulation has been set: $R_N = 10^{14}\,\frac{1}{\mathrm{m^3\,s}}$, $d_0 = 3\,\mathrm{nm}$. A monodisperse population with an initial concentration of $10^{17}\,\frac{1}{\mathrm{m^3}}$ has been used as start condition, the initial MC particles are equally weighted. The temperature was set to 300 K and the particle density to $1\,\frac{\mathrm{g}}{\mathrm{cm^3}}$. The simulated time was ca. 25.8 s, which is 500 times the characteristic time needed to reach the self-preserving distribution [28] due to coagulation.

Table 1 Values of the geometric mean diameter and simulation times (CPU time) for the discrete sectional (DS) method and MC simulations using Random removal (RR) and Low weight Merging (LWM) with 1000 and 10,000 MC particles

Method	Mean value d_g [nm]	Standard deviation Δd_g (absolute) [nm]	$100\Delta d_g/d_g$ (percent) [–]	CPU time [s]
DS (20 100)	4.736	–	–	8.4
DS (250 380)	4.740	–	–	332.1
RR 1000	4.820	0.544	11.29	330.3
RR 10,000	4.736	0.180	3.79	3964.2
LWM 1000	4.733	0.100	2.11	300.4
LWM 10,000	4.742	0.033	0.70	3643.2

The number of used sections and discrete points for DS are indicated by the values in the brackets (discrete points, sections). The exact 1D grid specifications are described in [23]

weight merging. It should also be noted that the computation of 10,000 MC particles requires ca. 10 times larger computing times than of 1000 particles. The computing times shown in Table 1 refer to the simulation of 100 MC simulations run in parallel on the GPU and one discrete-sectional run sequentially on the CPU.

2.3 Coupled Condensational Growth and Evaporation, Coagulation and Nucleation

A varying nucleation rate, R_N, as well as a changing critical nucleus size, d^*, is often encountered when a metallic vapor is created and then cools down, leading to the nucleation rate increasing over tens of orders of magnitude and then going down when the free atoms have been largely consumed. The size of the critical nucleus, d^*, on the other hand, decreases from very large values to atomic sizes, and rises again when the nucleation rate is increasing. This presents a severe test for the numerical solution, as the source term is moving rapidly through the size spectrum, leading to a dramatic change of the growth and evaporation rates of the simulated particles, as well. Hence particles larger than the nucleating particle (i.e. with volumes $v_i > v^*$) will grow, while those which are smaller (i.e. with volumes $v_i < v^*$) will evaporate. This is described by the equation of the growth-rate $G(v_i, N_G)$ of particles with the volumes v_i in the free-molecule regime [29]:

$$G(v_i, N_G) = \frac{\mathrm{d}v_i}{\mathrm{d}t} = \frac{v_M \cdot \pi \cdot d_i^2}{\sqrt{2\pi \cdot m_1 \cdot k_B \cdot T}} \cdot (k_B \cdot T \cdot N_G - p_s \cdot \exp\{4 \cdot \sigma \cdot v_M/(k_B \cdot T \cdot d_i)\}) \quad (10)$$

The value of the critical diameter is given by:

$$d^* = 4 \cdot \sigma \cdot \upsilon_\mathrm{M}/(k_\mathrm{B} \cdot T \cdot \ln(S)) \quad \text{with} \quad S = \frac{N_\mathrm{G} k_\mathrm{B} T}{p_\mathrm{S}} \tag{11}$$

So that $G(v_i, N_\mathrm{G}) = 0$ for $v_i = v^*$ and $G(v_i, N_\mathrm{G}) > 0$ for $v_i > v^*$. The growth rate of the particles is also dependent on the number of atoms (or molecules) of the condensable material in the gaseous phase, N_G. The depletion (resp. increase) of the monomers due to condensation on (resp. evaporation of) the particles is described by a mass balance:

$$\frac{\mathrm{d}N_\mathrm{G}}{\mathrm{d}t} = -\sum_i W_i \cdot G(v_i, N_\mathrm{G})/v_\mathrm{M} - R_\mathrm{N} \cdot i^* \tag{12}$$

Thereby, the nucleation of particles is also taken into account by the nucleation rate R_N and the number of atoms (resp. molecules) i^* in a particle of the critical size d^*.

We proposed an operator-splitting based approach for the parallel solution of this system [26, 27, 30], by decoupling the growth-evaporation and nucleation mechanism from the coagulation mechanisms for short periods of time, like in the presented coupled simulation of coagulation and nucleation in Sect. 2.2.3. The condensational growth (resp. evaporation) of the simulated particles is solved in parallel by application of time-step adaptive Runge-Kutta techniques (see e.g. [31]). A parallel addition algorithm, similar to the presented parallel comparison algorithm in Fig. 4, is used for the fast calculation of the term $\sum_i W_i \cdot G(v_i, N_\mathrm{G})$ in Eq. (12). A more detailed description of this approach can be found in [30]. This modelling of the continuous PSD with discrete MC particles avoids the effect of numerical diffusion [32, 33], encountered in models describing particle growth, in analogy to moving grid techniques for sectional methods [34].

It has be shown, that all of the mentioned mechanisms (i.e. evaporation, condensation, nucleation and coagulation) have to be considered and that the omission of one of these mechanisms leads to severe deviations from the 'complete' system [26].

The thus introduced methodology can be used to determine the influence of different formulations of nucleation rates and allows to identify experimental conditions for the experimental investigation of those. There exist several approaches for the description of nucleation theories [35]. We consider in the following these three expressions for the nucleation rate R_N, as discussed in [36]:

$$R_\mathrm{N}^{(\mathrm{cou})}(N_\mathrm{G}) = N_\mathrm{G} \cdot \sqrt{\frac{2\sigma}{\pi \cdot m_1} \frac{p_\mathrm{s}}{k_\mathrm{B} \cdot T}} \cdot v_1 \cdot \exp\left(-\frac{16 \cdot \pi \cdot \sigma^3 \cdot v_\mathrm{M}^2}{3 \cdot k_B^3 \cdot T^3 \cdot \ln(S)^2}\right),$$

Table 2 Material constants for Ag at a temperature of 1300 K

Symbol	Description	Value	Source
m_1	Atomic mass	1.792×10^{-25} kg	[37]
v_M	Atomic volume	1.922×10^{-29} m^3	[37]
p_s	Vapor pressure	1.324 pa	[37]
σ	Surface tension	0.9024 J/m^2	[38]

$$\text{with} \quad S = \frac{N_G k_B T}{p_s} \tag{13}$$

$$R_N^{(gir)}(N_G) = R_N^{(cou)} \cdot \exp\left((36 \cdot \pi)^{\frac{1}{3}} \cdot \frac{\sigma \cdot v_1^{\frac{2}{3}}}{k_B \cdot T} \right); \quad R_N^{(cls)}(N_G) = R_N^{(cou)} \cdot S \tag{14}$$

The influence of these different nucleation theories has been discussed for atmospheric simulation scenarios [27] and are briefly sketched for a metallic system describing the nucleation of Ag vapor in the following. The material parameters in Eqs. (10–14) assume values summarized in Table 2 at a temperature of $T = 1300$ K.

The simulation of a isothermal nucleation induced due to an initial supersaturation of $S_0 = 100$ of Ag vapor and the presence of an initial (background) PSD with a mean geometric diameter of 2 nm and a geometric standard deviation of 1.2 rendering a total number-concentration of 10^{16} m^{-3} is used as an initial condition. The temperature is kept constant to 1300 K during the course of the simulation.

The monomer concentration exhibits the fastest depletion rate for the Girshick-based nucleation rate, as is shown in Fig. 5a. This is due the highest nucleation rate which is plotted in comparison with other nucleation theories in Fig. 5b. This leads in turn to the highest particle concentrations for the Girshick-based nucleation theory (see figure Fig. 5c). The nucleation theories show the most striking differences at the early stages of the simulation, for longer simulation times, (i.e. t > 0.01 s), similar

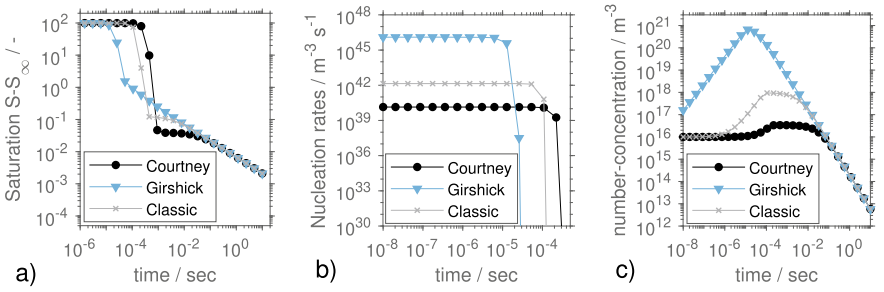

Fig. 5 Isothermal Ag particle synthesis with initial PSD and supersaturation $S_0 = 100$. The saturation surplus $S - 1$ (**a**), the corresponding nucleation rates (**b**) and the total particle number-concentrations (**c**) are shown. The nucleation rates $R_N^{(cou)}$ (Courtney) $R_N^{(gir)}$ (Girshick) and $R_N^{(cls)}$ (Classic) are defined in Eqs. (13) and (14)

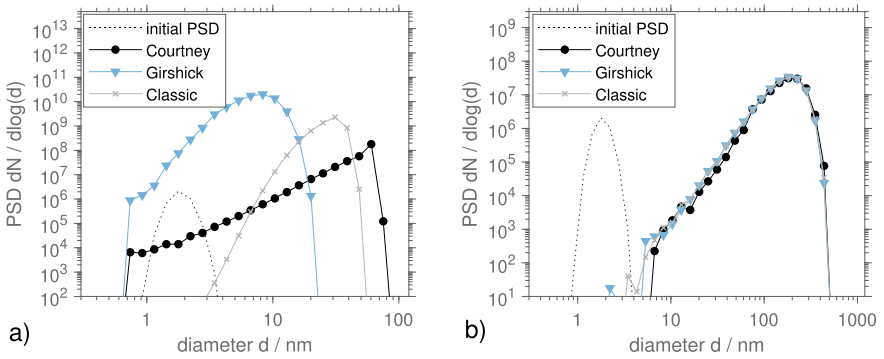

Fig. 6 Isothermal Ag particle synthesis with initial PSD and supersaturation $S_0 = 100$. Resulting PSDs after $2.2 \cdot 10^{-4}$s (**a**) and $1.4 \cdot 10^{-1}$s (**b**) for the nucleation rates $R_N^{(kin)}$ (Kinetic) $R_N^{(gir)}$ (Girshick) and $R_N^{(cou)}$ (Courtney) defined in Eqs. (13) and (14)

supersaturations and concentrations can be observed (in Fig. 5 a-c). This is a signature of the similar PSDs resulting from the simulation, as they are shown in Fig. 6.

The PSDs at the initial stages of the simulation (see Fig. 6a) show tremendous differences and allow to attribute each of the different shapes to a specific nucleation theory. For longer simulation times, on the other hand, a self-preserving PSD is reached and all of the presented nucleation theories can be attributed to the shown PSDs. The shown self-preserving PSD is the result of the complex coupling of the mechanisms of coagulation and evaporation. This PSD deviates from the self-preserving PSD for the coagulation only as reported Vemury and Pratsinis [28]. Similar self-preserving PSDs deviating from the self-preserving PSD for coagulation only have been already reported for similar metallic systems [26] and [30]. This approach allows thus to roughly approximate a time window, for which specific differences between the different nucleation rates can be expected. Allowing thus to give hints for measurements set-ups investigating the specific forms of the nucleation rate R_N.

2.4 Breakage

Breakage of particles is relevant for the modeling of particle mills, but also for granulation, emulsions, sprays and even for aerosols when agglomerates break up by collisions or turbulences. The rendering of the large number of particles which are produced during the continuous breakage process poses a major problem for MC simulations, because large computational resources have to be provided for this purpose. In a typical milling process, for example, reductions of the particle diameters from 500 to 0.5 μm are encountered, the same amount of volume, which is rendered by one simulation particle with a size of 500 μm has to be rendered by

10^9 simulation particles with a diameter of 0.5 μm, if all particles represent the same number concentration of real particles.

Traditional solutions of this problem encompass the discretization of the particle property into bins [39], which would render the combination with the developed growth/evaporation algorithm impossible, and constant-number approaches [40], which are known to produce a high level of statistical noise [41].The application of merging schemes [42] (i.e. the approximation of the properties of several simulation particles by one simulation particle) would pose an attractive alternative. However, the vast amount of newly resulting particles makes a lot of merging steps necessary, leading to large computing times. A recent constant-number method has been presented [41], which renders the breakage event of one particle into many fragments by a single particle. The size of the fragment is selected stochastically, the use of many simulation particles leads to the correct distribution of fragment sizes. This scheme is only able to render the parts of the particle size distribution which represent high number concentrations of the particles. Furthermore, only binary breakage can be described.

We developed an alternative approach [43] for the derivation of the breakage scheme by resorting to the argument that the breakage of many MC-particles with equal properties and weights has to lead to a particle size distribution (PSD) of fragments, which is described by the corresponding breakage kernel. It allows to formulate any probability distribution function (PDF) with which the new volume of the simulation particle is selected by adjusting the statistical weight of the resulting fragments depending on 1) the selected particle properties, 2) the used PDF and 3) the given breakage density function. This newly proposed scheme encompasses the already introduced SWA schemes, especially a number-based (NB, named SWA1 in [41]) and volume-based (VB, named SWA2 in [41]) breakage scheme, and it makes novel formulations possible: the low volume scheme (LV), which renders preferably fragment particle sizes at the lower end of the size spectrum, and the combination of LV with the NB (NB-LV) or VB (VB-LV). Exemplary simulation results are shown in Fig. 7. It can be seen that the SWA methods (NB and VB) are only able to render large particle sizes, and that LV, NB-LV and VB-LV are able to render the whole spectrum of particle sizes. Smaller noise levels are found for VB and specific VB-LV schemes, making both more suitable for prolonged simulations than the other presented methods. The LV based simulation method fails to predict the correct PSDs for longer simulation times. For this reason, the combinations of LV with VB or NB are needed, in order to ensure the correct shapes of the PSDs for longer simulation times. The combination ratio $R \in (0, 1)$ between the LV and NB leads to different schemes, while lower ratios R lead to a higher representation of low-volume MC particles, they also lead to higher noise levels: the setting $R = 0.6$ leads to more statistical noise than $R = 0.9$, as it can be seen in Fig. 7. The adaptive resetting of the factor R in order to avoid the systematical errors, as it is shown in Fig. 7 for the LV scheme is briefly discussed in [44].

The required simulation times are listed in Table 3, 10^5 simulation particles are required in order to ascertain a computational accuracy of less than 1%. (I.e. the

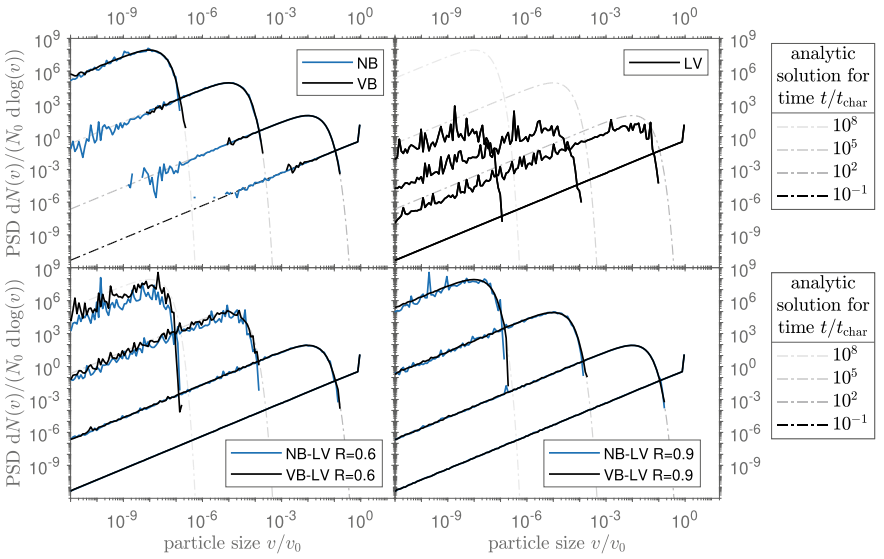

Fig. 7 Resulting PSDs from the simulation of a test cases describing a binary, homogeneous particle breakage function $\gamma(v_{\mathrm{F}}, v_{\mathrm{P}}) = 2/v_{\mathrm{P}}$ and a breakage rate $b(v) = v$ (test case 1 in [43]) for a monodisperse initial condition v_0 and the thus defined characteristic time $t_{\mathrm{char}} = b(v_0)^{-1}$. The MC-simulations are compared with analytic solutions found in [46]

Table 3 Computational times required for the simulation of $t = t_{\mathrm{char}} \times 10^8$ in dependency on the used number of simulation particles

Simulation particles	NB	VB	VB-LV
1000	0.5 s	0.8 s	0.6 s
10,000	2.8 s	4.4 s	3.0 s
100,000	27.1 s	42.5 s	29.8 s

arithmetic standard deviation of the moments of the distributions performed for 100 different sets of random numbers is smaller than 1% of the mean value.)

3 Compartmental Population Balance Modelling

The modelling of flow-sheet simulations in the scope of an operator-splitting approach (see e.g. [47]) requires a specific time step management, so that ongoing simulations processes can be forced to stop at specific simulation time points. This issue is addressed first, in a second, longer paragraph, the implementation of particle transport between single compartments by means of weighted MC particles is introduced and some typical simulation scenarios are presented.

3.1 Time Step Control for Compartmental PBE Networks

The combination of simultaneous processes rendered by the PBE solver poses a challenging task, hence the characteristic time-scales for the corresponding processes may differ in several orders of magnitude and change vastly during the simulation. Although the developed algorithms for the breakage, coagulation and growth (resp. evaporation) already adapt to the optimal time-step for each single process (in the absence of other processes), the simulation of the combined coagulation, nucleation and growth is driven by the discrete coagulation processes providing an inherent MC time step τ_{MC}. This is a computationally advantageous setting, if the inherent growth step τ_{G} is smaller than the coagulation step τ_{MC}. The opposite case, in which τ_{G} is bigger than τ_{MC}, forces the simulation to use much smaller time steps τ'_{G} and thus to use much more computationally demanding growth steps. The incorporation of the breakage as a third process with an inherent time step τ_{B} may force the simulation to reset this step to a lower value τ'_{B} in a coagulation driven implementation, as well.

This situation becomes even more complicated, if the PBE is solved for different compartments and a particulate flow between the compartments is simulated. Consider, for example two compartments, in which coagulation takes place, so that compartment 1 has an intrinsic MC coagulation time step $\tau_{\mathrm{MC}}^{(C1)}$, while the second compartment has the inherent coagulation time step $\tau_{\mathrm{MC}}^{(C2)}$, the additional particulate flowrate between compartment 1 and compartment 2 might make the update of the particle populations due to the transport of particles each time interval τ_{Tr} necessary. It depends on the specific modelled application, whether the minimum of these three time steps has to be used, or some other minimal time step τ_{min} can be applied. In all cases, there exists the need, to perform, at least in one of the two compartments, a smaller time step than the one intrinsically provided ($\tau_{\mathrm{MC}}^{(C1)}$ and/or $\tau_{\mathrm{MC}}^{(C2)}$).

The application of time-driven MC methods [48] allows the setting of a variable time step, but this time step has to be set proportional to the intrinsic step in order to avoid systematical errors [49], although smaller values are allowed. The main disadvantage of this approach is, however, its computational costs, hence all possible coagulation pairs have to be checked for coagulation during the suggested time step—special book-keeping methods [50] might help to address this problem for the single simulation of coagulation but their usage is not possible[2] in the context of a PBE network modelling multiple simultaneous processes.

We have developed the concept of 'fractional MC time steps' [51], in order to address this problem. In the scope of this approach, we modified the fast GPU acceptance-rejection algorithm [25] in such a way, that an additional stochastic probability is formulated, whether the particles coagulate or not if a smaller time step than the intrinsic MC AR-time step is needed. We compared our methodology (marked

[2]Special modeling is necessary in order to capture the changes of the 'book kept' entries due to other non-coagulation processes—this might or might not be possible, depending on the specific process being modelled. Additionally, the tracking of the changes might prove more expensive than the application of the time-driven MC methods without book-keeping.

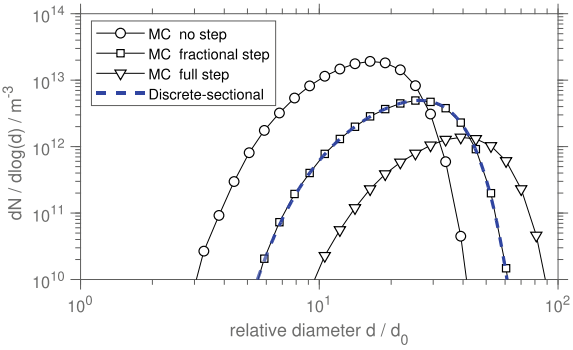

Fig. 8 PSDs resulting from simulation conditions as described in [51]

as 'MC full step') with (1) another approach from the literature [21], where no coagulation of the particles takes place in such an event (marked as 'no step') and (2) with the self-proposed approach, where the particles simply coagulate—even if the simulated time step is smaller than the intrinsic time step (marked as 'full step'). A typical isothermal coagulation scenario describing Brownian motion of particles in the free-molecule regime (full details can be found in [51]), leads to the following simulation results shown in Fig. 8, if the simulated system is forced to perform not the intrinsic MC time steps but an artificial time step of 1 ms. It can be clearly seen, that only the application of the fractional MC time steps leads to the correct description of the PSDs, which is in excellent agreement with the reference result gained by the application of the discrete-sectional method, as described in [52, 53].

3.2 Compartmental Monte Carlo Simulation

Modelling of MC particle transport as a stochastic process with discrete events is sometimes suggested [54]. Such a modelling, could—however— entail a large number of stochastic events for small simulation times and slow down the simulation considerably. The other disadvantage of such an approach is the potential increase of the stochastic noise of the simulation.

The description of weighted simulation particles makes novel simulation strategies for the transport possible, the adjustment of the statistical weight of each MC particle makes the exact description of the depletion of particles due to particle outflow possible—as is discussed in [20] (termed 'rescale outflow') and shown in the following. First, the description of a two-step (inflow and outflow) method is suggested and the merging and random removal techniques are briefly described, then the methodologies are validated and compared by simulations of exemplary flowsheets.

3.2.1 Transport of Weighted MC Particles

In the following, the transport of MC particles from one compartment to other compartments will be described. It consists of two steps: (1) the particle outflow and (2) the particle inflow. This is being realized by the computational implementation of 'streams' which are able to store a population of MC particles, as large as the population stored for each compartment.

In the first outflow step, particles are inserted into the streams. This can be easily done by copying all particles from the hold-up into the stream and adjusting the statistical weights accordingly, in the stream and in the hold-up. If, for example, the particles from compartment 1 stream into compartment 2 with the size v dependent relative rate $f_{1\to 2}(v)$, then one can describe for each particle i the change of its statistical weight W_i for a small interval of time Δt as:

$$W_i(t+\Delta t) = W_i(t) - \Delta t \cdot f_{1\to 2}(v_i) \cdot W_i(t) \tag{15}$$

This is shown as particle outflow step in Fig. 9. The new weights W_i^{s1} and $\overline{W}_i^{c1}$ are set to $W_i^{s1} = \Delta t \cdot f_{1\to 2}(v_i) \cdot W_i^{c1}$ and $\overline{W}_i^{c1} = W_i^{c1} - W_i^{s1}$.

In the inflow step in Fig. 9, the particles from the streams are inserted into the compartments. Analogously to the already discussed nucleation of particles, one encounters at this step the problem of the limited CPU memory: each connecting stream contains as many particles as the destination compartment, so that only a fraction of all MC particles can be stored in the destination compartments. This problem has been solved in two ways in the here presented work: (1) randomly selected particles are removed from the simulation—adjusting the statistical weights in such a way, that the mass of the system remains constant as in the conventionally used constant number algorithms [55, 56] and (2) the particles are merged together using a parallel merge algorithm as it is briefly discussed in [57].

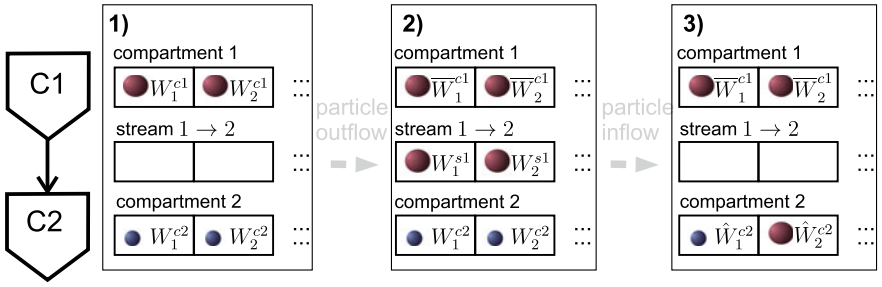

Fig. 9 MC particles stored in the memory assigned for compartment 1 and 2, as well as in the stream connecting both compartments. The stages (1) before the particle outflow (2) between outflow and inflow and (3) after the inflow during the simulation of a single time step are shown

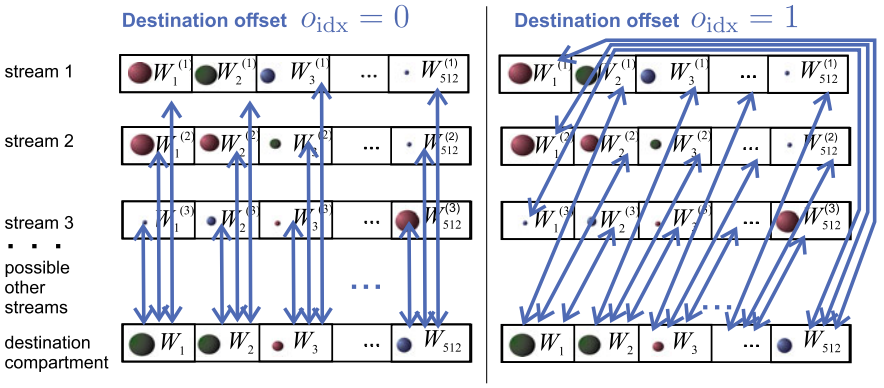

Fig. 10 Compartment-Stream merge pattern. Each double arrow represents one merge attempt. All merge attempts which are executed in parallel with the destination offset $o_{\mathrm{idx}} = 0$ are shown in comparison with all parallel merge attempts made for the offset $o_{\mathrm{idx}} = 1$

3.2.2 Parallel Merge Algorithm

The merging algorithm described in Fig. 4 could be used for the merging of MC particles within stream and the destination compartment. However, such an approach would be computationally not efficient due to the large number of MC particles ranging in typical applications between 1000 and 10000. This would imply 1000 or 10000 sequential or parallel invocations of the algorithm presented in Fig. 4. In order to accelerate the merging process, a novel parallel algorithm has been briefly sketched in [57] and is discussed here in more detail. The GPU's capability to process a large amount of data in parallel can be exploited in a more efficient way, if not only one (as in Fig. 4) but a large number of MC particles has to be merged together (as in Fig. 9).

The merging scheme described by Eq. (6) and (7) can be thereby used in combination with the merging error described by Eq. (9). A maximal admittable merging error ε can be formulated and all particle pairs (i, j) with a merging error $E_{i,j}$ (Eq. (9)) smaller than ε are merged together. A large number of parallel comparisons can thereby be performed, forming potential pairs for the merging by calculation of the merging errors of the pairs consisting of one particle in the destination compartment and one particle in one of the streams, as shown as 'Compartment-stream merge pattern' in Fig. 10. The destination offset, o_{idx}, is thereby increased by one after each comparison attempt, so that different pairs are formed for the calculation of the merging error. After 512 steps, all possible pairs between each of the compartment particle and another stream MC particle would have been checked in this way.[3] An internal check between particles stored in the compartment (resp. streams) is also

[3] In order to use the GPU efficiently, larger particle numbers (like e.g. 10000) have to be divided into data blocks consisting of e.g. 512 particle numbers. In the here presented implementation, particle numbers that are multiples of 512 are considered.

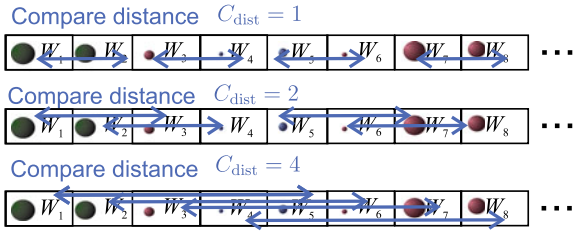

Fig. 11 Intern merge pattern. All merge attempts which are executed in parallel within one stream or compartment with different compare distances C_{dist}

performed, in order to address situations, in which the populations in the streams are so different from the population in the compartment, that a merging is only possible with very high merging errors. These 'internal merges' are shown in Fig. 11. The multiplication of the compared distance C_{dist} with the factor of 2, ensures the treatment of different pairs after each invocation of the routine.

The complete algorithm for the parallel merging is shown in Fig. 12, the following settings are set arbitrarily:

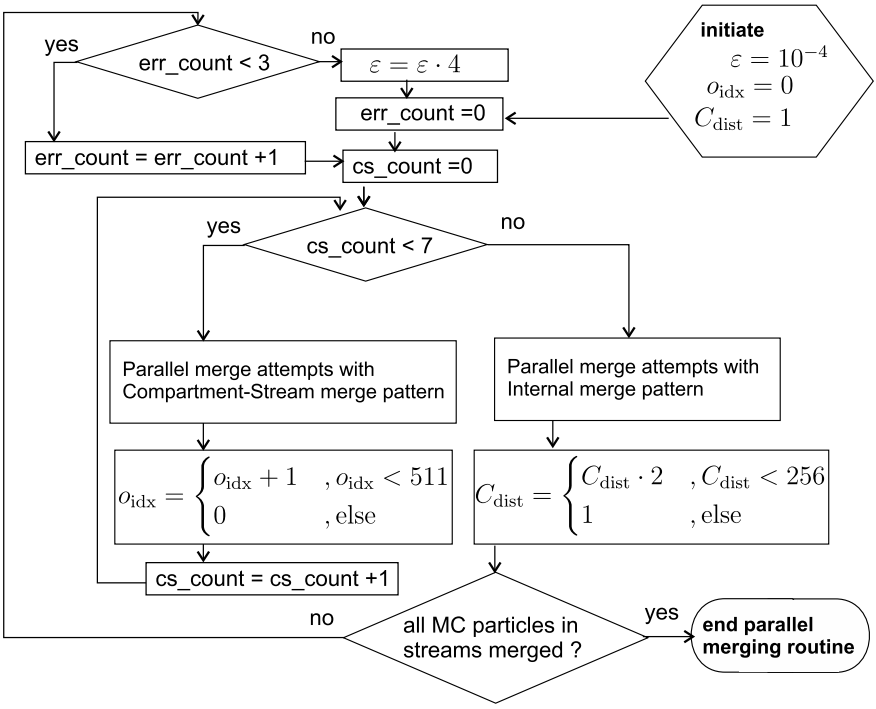

Fig. 12 Sketch of the merge algorithm for MC particle insertion. The Compartment-Stream merge pattern is shown in Fig. 10 and the internal merge pattern is shown in Fig. 11

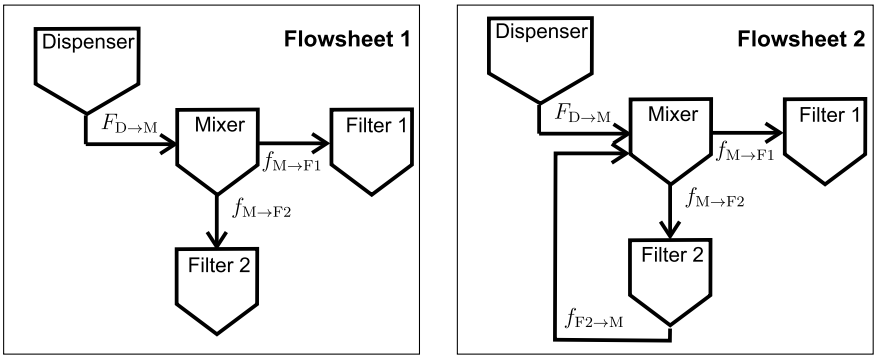

Fig. 13 Exemplary flow-sheets with and without a feedback stream

- 8 Compartment-Stream merge patterns are performed for each invoked intern merge-pattern ('cs_count < 7' in Fig. 12). This combination is invoked each time before the (rather costly) check if all particles have been merged is initiated.
- After each 4 unsuccessful checks if all particles have merged, the maximal admittable merging error is increased ('err_count < 3' in Fig. 12).
- The maximal admittable merging error is increased by a factor of 4 ('$\varepsilon = \varepsilon \cdot 4$').

These settings prove to work efficiently for the presented test cases in the validation section. Other settings might be more appropriate for other application scenarios and the dynamic adaptation of these values to given simulation conditions might pose an interesting research topic for future investigations.

3.2.3 Validation

The proposed simulation techniques are validated on several test-cases, which reflect simple engineering problems and are shown in the figures Figs. 13 and 14. The shown flowsheets increase in complexity, hence the implementation of a tear stream (Flowsheet 2, Fig. 13) or a sieve unit (Flowsheet 3, Fig. 14) or both in combination (Flowsheet 4, Fig. 14) poses a greater challenge for the numerical solution than the simple flowsheet 1 in Fig. 13. This methodology allows to identify the specific simulation scenario, for which conventional MC strategies are not suitable and the here presented methodology based on weighted MC particles has to be applied in order to obtain correct results.

For each of the presented units in Fig. 13, the evolution of the PSDs n_{M} (mixer), n_{F1} (filter 1) and n_{F2} (filter 2) can be modelled by the explicit set of differential equations:

$$\begin{aligned}\frac{\mathrm{d}n_{\mathrm{M}}(v,t)}{\mathrm{d}t} &= + f_{\mathrm{F2}\to\mathrm{M}} \cdot n_{\mathrm{F2}}(v,t) - f_{\mathrm{M}\to\mathrm{F1}} \cdot n_{\mathrm{M}}(v,t) - f_{\mathrm{M}\to\mathrm{F2}} \cdot n_{\mathrm{M}}(v,t) \\ &\quad + F_{\mathrm{D}\to\mathrm{M}} \cdot n_{\mathrm{D}}(v,t)\end{aligned}$$

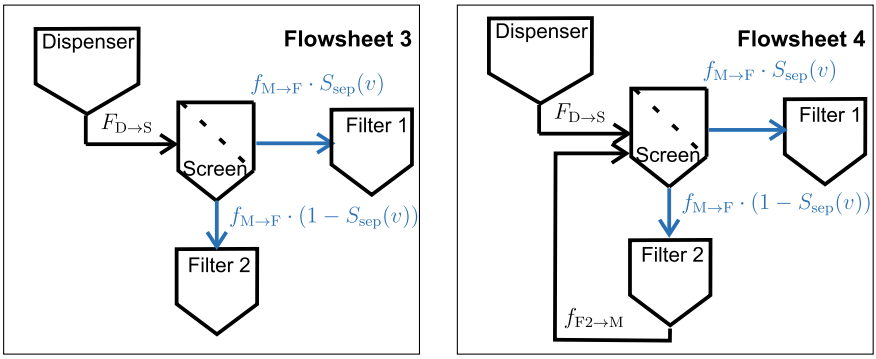

Fig. 14 Exemplary flow-sheets with and without feedback including a feedback stream

$$\begin{aligned} \frac{\mathrm{d}n_{F1}(v,t)}{\mathrm{d}t} &= +\, f_{M\to F1} \cdot n_M(v,t) \\ \frac{\mathrm{d}n_{F2}(v,t)}{\mathrm{d}t} &= +\, f_{M\to F2} \cdot n_M(v,t) - f_{F2\to M} \cdot n_{F2}(v,t) \end{aligned} \tag{16}$$

The relative particle exchange rates $f_{A\to B}$ from unit A to unit B are multiplied with the particle PSDs in A, n_A, which change over time. The external particle exchange rate $F_{D\to M}$ is multiplied with a PSD, n_D, which does not change in time, realizing thus in a constant in-flow into the mixer unit. The explicit values for the exchange rates used for these benchmarking test cases are summarized in Table 4.

The system in Fig. 13 described by Eq. (16) does not take specific particle sizes v into account, so that the same particle exchange rates apply for all sizes v. The application of a screen unit changes this situation, so that the total particle exchange rate from the screen to both filters, $f_{S\to F}$, is multiplied with the separator function, $S_{sep}(v)$. This leads to the following set of equations for the flowsheets shown in Fig. 14:

Table 4 Particle exchange rates for Eqs. (16) and (17)

	Flowsheet 1 in Fig. 13	Flowsheet 2 in Fig. 13	Flowsheet 3 in Fig. 14	Flowsheet 4 in Fig. 14
$F_{D\to M}$ or $F_{D\to S}$ [1/s]	3	3	3	3
$f_{M\to F1}$ [1/s]	1	1	–	–
$f_{M\to F2}$ [1/s]	2	2	–	–
$f_{M\to F}$ [1/s]	–	–	3	3
$f_{F2\to M}$ or $f_{F2\to S}$ [1/s]	0	2	0	2

$$\begin{aligned}
\frac{\mathrm{d}n_{\mathrm{S}}(v,t)}{\mathrm{d}t} &= +f_{\mathrm{F2}\to S}\cdot n_{\mathrm{F2}}(v,t) - f_{\mathrm{S}\to\mathrm{F}}\cdot n_{\mathrm{M}}(v,t) + F_{\mathrm{D}\to\mathrm{S}}\cdot n_{\mathrm{D}}(v,t)\\
\frac{\mathrm{d}n_{\mathrm{F1}}(v,t)}{\mathrm{d}t} &= +f_{\mathrm{S}\to\mathrm{F}}\cdot n_{\mathrm{S}}(v,t)\cdot S_{\mathrm{sep}}(v)\\
\frac{\mathrm{d}n_{\mathrm{F2}}(v,t)}{\mathrm{d}t} &= +f_{\mathrm{S}\to\mathrm{F}}\cdot n_{\mathrm{S}}(v,t)\cdot(1-S_{\mathrm{sep}}(v)) - f_{\mathrm{F2}\to S}\cdot n_{\mathrm{F2}}(v,t)
\end{aligned} \tag{17}$$

The explicit particle exchange rates for these equations are summarized in Table 4. The following form of the separation function $S_{\mathrm{sep}}(v)$ has been used for the screen:

$$S_{\mathrm{sep}}(v) = \begin{cases} 1, & v > v_{\mathrm{max}}^{\mathrm{sep}} \\ (v - v_{\mathrm{min}}^{\mathrm{sep}})/(v_{\mathrm{max}}^{\mathrm{sep}} - v_{\mathrm{min}}^{\mathrm{sep}}), & v_{\mathrm{max}}^{\mathrm{sep}} > v > v_{\mathrm{min}}^{\mathrm{sep}} \\ 0, & v_{\mathrm{min}}^{\mathrm{sep}} > v \end{cases} \tag{18}$$

The separation cut-off values $v_{\mathrm{max}}^{\mathrm{sep}} = \pi(d_{\mathrm{max}}^{\mathrm{sep}})^3/6$ and $v_{\mathrm{min}}^{\mathrm{sep}} = \pi(d_{\mathrm{max}}^{\mathrm{sep}})^3/6$ correspond to the diameters $d_{\mathrm{max}}^{\mathrm{sep}} = 57$ nm and $d_{\mathrm{min}}^{\mathrm{sep}} = 40$ nm.

As initial conditions for the PSDs in the mixer $n_{\mathrm{M}}^0(v)$ (resp. screen $n_{\mathrm{S}}^0(v)$), two identic log-normal distributions with a geometric mean diameter of 50 nm, a geometric standard deviation of 1.2 and a total number-concentration of $10^{10}\mathrm{m}^{-3}$ have been used. The same distribution has been used as feed PSD, i.e. $n_{\mathrm{D}}(v)$. Both filters are empty at the beginning of the simulation ($n_{\mathrm{F1}}^0(v) = n_{\mathrm{F2}}^0(v) = 0$).

A fixed pivot method [58] has been used as benchmark. The continuous initial PSDs are thereby discretized with the help of a geometric grid of 1000 pivot points, covering a particle size range from 1 nm to 10 µm. In the scope of this approach, the set of Eqs. (16) or (17) is interpreted as the rate of change for each single pivot point with its respective volume v.

The resulting PSDs after a simulation time of 10 s are shown in Figs. 15, 16, 17, 18. It can be seen, that flowsheet 1 (without tear streams and a screen) is very well

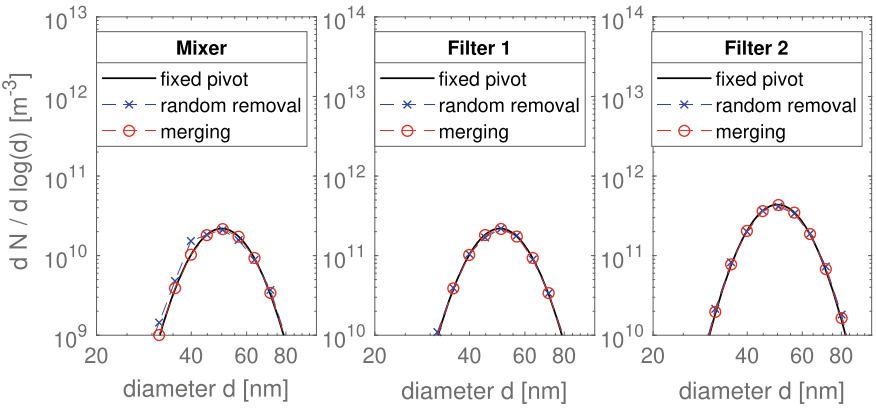

Fig. 15 PSDs in compartments as described in Flowsheet 1 in Fig. 13 and Eq. (16)

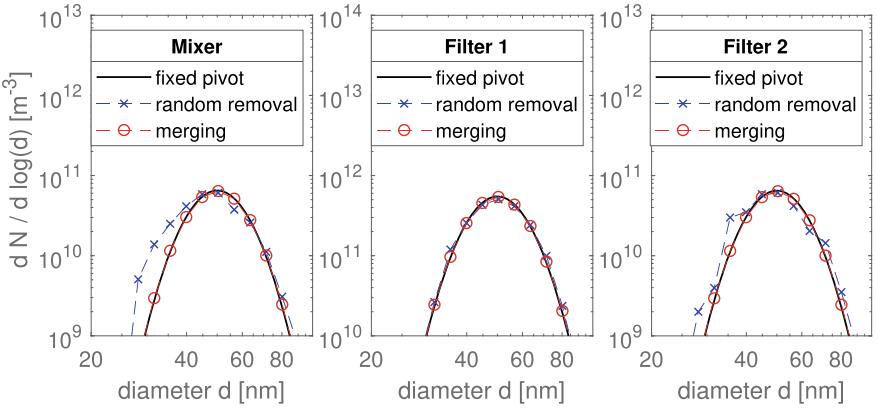

Fig. 16 PSDs in compartments as described in Flowsheet 2 in Fig. 13 and Eq. (16)

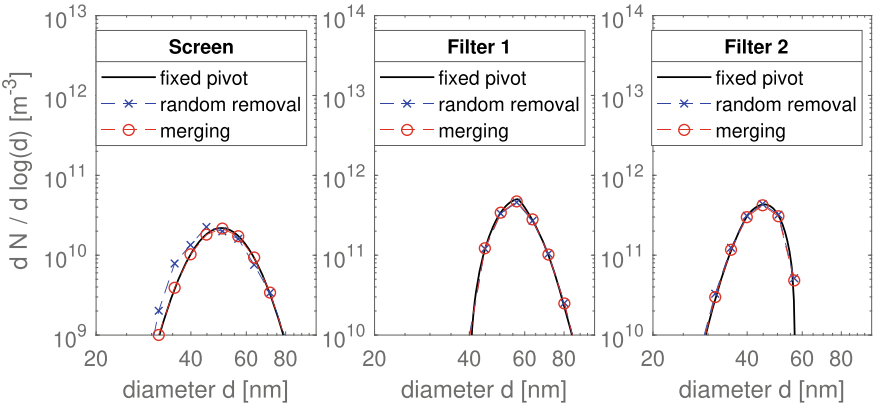

Fig. 17 PSDs in compartments as described in Flowsheet 3 in Fig. 14 and Eq. (17)

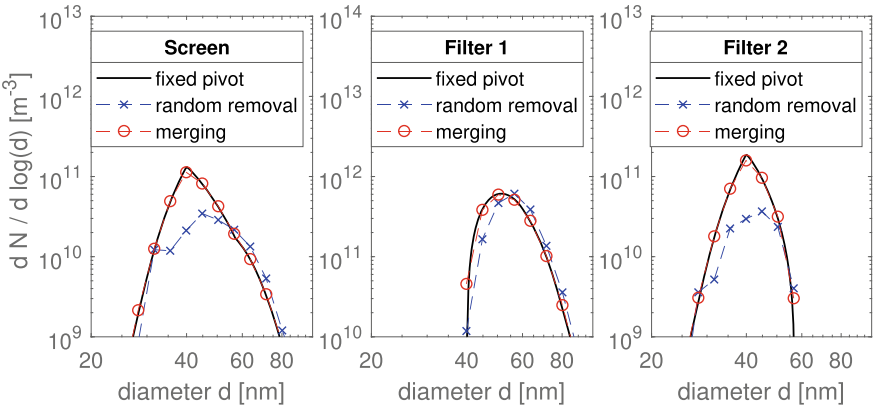

Fig. 18 PSDs in compartments as described in Flowsheet 4 in Fig. 14 and Eq. (17)

reproduced by the merging as well as the random removal approach. The random removal approach leads to larger noise levels, which can be seen in slight deviations of the PSD in the mixer unit in Fig. 15. The addition of a tear stream leads to an increase of these noise levels, as can be seen Fig. 16—the approximations based on the random removal technique become less accurate but can be still considered to be in accordance with the results obtained by the fixed pivot method.

The replacement of the mixer with a sieve unit (or replacing flowsheet 1 with flowsheet 3) leads also to a system, which can be well simulated by the random removal technique (see Fig. 17). The addition of a tear stream to flowsheet 3 (resulting in flowsheet 4) leads—however—to such a complex system, that the random removal method is not applicable. Figure 18 shows the striking deviations of the PSDs obtained with the random removal method—which predict a wrong particle-number concentration in the screen and filter 2 by a factor of nearly 10. The suggested merging techniques—on the other hand—are able to reproduce the benchmark results with a very high accuracy. This allows to say, that the specific combination of tear-stream and screen leads to a simulation scenario, which cannot be addressed with conventional MC simulation techniques—as the random removal technique. This finding also explains the failure of the random removal techniques to describe an even more complex simulation scenario, reported in [57].

4 Conclusions

The application of weighted MC particles for the solution of a compartmental network in the framework of an operator splitting approach (the single processes like coagulation and nucleation are separated for short periods of time) has been discussed.

First, the solution of a one-compartmental system has been discussed, it has been found that:

- the application of the stochastic resolution allows to describe the coagulation between weighted simulation particles (like already discussed in [23]).
- merging techniques allow to simulate the combined nucleation and coagulation with a lower amount of statistical noise than conventional MC simulation techniques (like already discussed in [23]).
- the parallel simulation of evaporation and condensational growth allows to simulate particles formation processes and investigate the role of different nucleation theories (this has been already discussed for metallic [26] and atmospheric systems [27], but the here presented case-study of Ag-particle synthesis has not been published prior to this work).
- novel selection and weighting techniques of the MC fragment population resulting from particle breakage lead to simulation techniques which are able to render the full particle size spectrum completely (these simulation techniques and findings have already been presented in [43]).

As a second step, the combination of the findings above in an operator splitting approach for the full simulation of a compartmental network has been sketched. It has been found that:

- the computationally advantageous event-driven simulation technique can be also used for the simulation of smaller time steps than the intrinsic MC time step—making this method applicable for a network of PBE compartments (like already discussed in [51]).
- the merging techniques introduced in [23] can be used for the simulation of particle transport between single compartments. (These findings have already been presented on a more complicated system in [57], the here presented description of the simulation algorithm is, however, far more detailed.)
- out of 4 case studies of a flow-sheet with increasing degree of complexity,[4] conventional MC methods can simulate the 3 simplest cases while merging techniques are needed for the simulation of the most complex case (this finding has not been published prior to this work).

Acknowledgements This work is supported by the DFG (Deutsche Forschungsgemeinschaft) within the priority program SPP 1679 "Dynamic flowsheet simulation of interconnected solids processes" [KR 1723/15–1,2&3].

References

1. Ramkrishna, D.: In: Population Balances: Theory and Applications to Particulate Systems in Engineering, 1st edn., Academic (2000). ISBN 978–0-12-576970-9
2. Ramkrishna, D., Singh, M.R.: Population balance modeling: current status and future prospects. Ann. Rev. Chem. Biomol. Eng. **5**, 123–146 (2014)
3. Schwarzer, H.-C., Peukert, W.: Combined experimental/numerical study on the precipitation of nanoparticles. AIChE J. **50**(12), 3234–3247 (2004)
4. Sommer, M., Stenger, F., Peukert, W., Wagner, N.J.: Agglomeration and breakage of nanoparticles in stirred media mills—a comparison of different methods and models. Chem. Eng. Sci. **61**(1), 135–148 (2006)
5. Peglow, M., Kumar, J., Heinrich, S., Warnecke, G., Tsotsas, E., Mörl, L., et al.: A generic population balance model for simultaneous agglomeration and drying in fluidized beds. Chem. Eng. Sci. **62**(1–2), 513–532 (2007)
6. Kraft, M.: Modelling of particulate processes. KONA Powder Particle J. **23**, 18–35 (2005)
7. Kiparissides, C.: Challenges in particulate polymerization reactor modeling and optimization: a population balance perspective. J. Process. Control. **16**(3), 205–224 (2006)
8. Bhole, M.R., Joshi, J.B., Ramkrishna, D.: CFD simulation of bubble columns incorporating population balance modeling. Chem. Eng. Sci. **63**(8), 2267–2282 (2008)
9. Schütz, S., Gorbach, G., Piesche, M.: Modeling fluid behavior and droplet interactions during liquid–liquid separation in hydrocyclones. Chem. Eng. Sci. **64**(18), 3935–3952 (2009)

[4]The four case studies comprise: (1) a flowsheet without recycle stream and screen units, (2) a flowsheet with one recycle stream and without sieve unit, (3) a flowsheet with one sieve unit and without recycle stream and (4) a flowsheet with a recycle stream and a sieve unit.

10. Sanyal, J., Marchisio, D.L., Fox, R.O., Dhanasekharan, K.: On the comparison between population balance models for CFD simulation of bubble columns. Ind. Eng. Chem. Res. **44**(14), 5063–5072 (2005)
11. Cheng, J., Yang, C., Jiang, M., Li, Q., Mao, Z.-S.: Simulation of antisolvent crystallization in impinging jets with coupled multiphase flow-micromixing-PBE. Chem. Eng. Sci. **171**, 500–512 (2017)
12. Marchisio, D.L., Fox, R.O.: Solution of population balance equations using the direct quadrature method of moments. J. Aerosol Sci. **36**(1), 43–73 (2005)
13. Gavi, E., Marchisio, D.L., Barresi, A.A.: CFD modelling and scale-up of Confined Impinging Jet Reactors. Chem. Eng. Sci. **62**(8), 2228–2241 (2007)
14. Boje, A., Akroyd, J., Sutcliffe, S., Edwards, J., Kraft, M.: Detailed population balance modelling of TiO_2 synthesis in an industrial reactor. Chem. Eng. Sci. **164**, 219–231 (2017)
15. Szilágyi, B., Nagy, Z.K.: Population balance modeling and optimization of an integrated batch crystallizer-wet mill system for crystal size distribution control. Cryst. Growth Des. **18**(3), 1415–1424 (2018)
16. Hao, X., Zhao, H., Xu, Z., Zheng, C.: Population balance-Monte Carlo simulation for gas-to-particle synthesis of nanoparticles. Aerosol Sci. Technol. **47**(10), 1125–1133 (2013)
17. Irizarry, R.: Stochastic simulation of population balance models with disparate time scales: hybrid strategies. Chem. Eng. Sci. **66**(18), 4059–4069 (2011)
18. Dosta, M., Heinrich, S., Werther, J.: Fluidized bed spray granulation: analysis of the system behaviour by means of dynamic flowsheet simulation. Powder Technol. **204**(1), 71–82 (2010)
19. Skorych, V., Dosta, M., Hartge, E.-U., Heinrich, S.: Novel system for dynamic flowsheet simulation of solids processes. Powder Technol. **314**, 665–679 (2017)
20. Menz, W.J., Akroyd, J., Kraft, M.: Stochastic solution of population balance equations for reactor networks. J. Comput. Phys. **256**, 615–629 (2014)
21. Kruis, F.E., Wei, J., van der Zwaag, T., Haep, S.: Computational fluid dynamics based stochastic aerosol modeling: combination of a cell-based weighted random walk method and a constant-number Monte-Carlo method for aerosol dynamics. Chem. Eng. Sci. **70**, 109–120 (2012)
22. Zhao, H., Kruis, F.E., Zheng, C.: Reducing statistical noise and extending the size spectrum by applying weighted simulation particles in Monte Carlo simulation of coagulation. Aerosol Sci. Technol. **43**(8), 781–793 (2009)
23. Kotalczyk, G., Kruis, F.E.: A Monte Carlo method for the simulation of coagulation and nucleation based on weighted particles and the concepts of stochastic resolution and merging. J. Comput. Phys. **340**, 276–296 (2017)
24. Lin, Y., Lee, K., Matsoukas, T.: Solution of the population balance equation using constant-number Monte Carlo. Chem. Eng. Sci. **57**(12), 2241–2252 (2002)
25. Wei, J.: A fast Monte Carlo method based on an acceptance-rejection scheme for particle coagulation. Aerosol Air Quality Research **13**(4), 1273–1281 (2013)
26. Kotalczyk, G., Skenderovic, I., Kruis, F.E.: Modeling of particle formation in arc discharges by Monte-Carlo based population balance modeling. MRS. Adv. **148**, 1–8 (2017)
27. Kotalczyk, G., Skenderovic, I., Kruis, F.E.: Monte Carlo simulations of homogeneous nucleation and particle growth in the presence of background particles. Tellus, Ser. B. Chem. Phys. Meteorol. **71**(1), 1–10 (2019)
28. Vemury, S., Pratsinis, S.E.: Self-preserving size distributions of agglomerates. J. Aerosol Sci. **26**(2), 175–185 (1995)
29. Kodas, T.T., Hampden-Smith, M.J.: Aerosol Processing of Materials, Wiley-VCH (1999). ISBN 0471246697
30. Kotalczyk, G., Skenderovic, I., Kruis, F.E.: A GPU-based Monte Carlo technique for the simulation of simultaneous nucleation, coagulation and growth based on weighted simulation particles. In: AIChE Annual Meeting, pp. 490–497 (2016)
31. Press, W.H.: In: Numerical recipes: The Art of Scientific Computing, 3rd edn. Cambridge University Press (2007). ISBN 978-0521880688
32. Tsang, T.H., Rao, A.: Comparison of different numerical schemes for condensational growth of aerosols. Aerosol Sci. Technol. **9**(3), 271–277 (1988)

33. Wu, C.-Y., Biswas, P.: Study of numerical diffusion in a discrete-sectional model and its application to aerosol dynamics simulation. Aerosol Sci. Technol. **29**(5), 359–378 (1998)
34. Kumar, S., Ramkrishna, D.: On the solution of population balance equations by discretization – III. Nucleation, growth and aggregation of particles. Chem. Eng. Sci. **52**(24), 4659–4679 (1997)
35. Wyslouzil, B.E., Wölk, J.: Overview: homogeneous nucleation from the vapor phase−the experimental science. J. Chem. Phys. **145**(21) (2016)
36. Girshick, S.L., Chiu, C.-P.: Kinetic nucleation theory: a new expression for the rate of homogeneous nucleation from an ideal supersaturated vapor. J. Chem. Phys. **93**(2), 1273–1277 (1990)
37. Lide, D.R. (ed.): CRC Handbook of Chemistry and Physics: A Ready-Reference Book of Chemical and Physical Data, 85th edn. CRC Press, Boca Raton (2004)
38. Egry, I., Ricci, E., Novakovic, R., Ozawa, S.: Surface tension of liquid metals and alloys-recent developments. Adv. Coll. Interface. Sci. **159**(2), 198–212 (2010)
39. Mishra, B.K.: Monte Carlo simulation of particle breakage process during grinding. Powder Technol. **110**(3), 246–252 (2000)
40. Lee, K., Matsoukas, T.: Simultaneous coagulation and break-up using constant-N Monte Carlo. Powder Technol. **110**(1–2), 82–89 (2000)
41. Lee, K.F., Patterson, R.I.A., Wagner, W., Kraft, M.: Stochastic weighted particle methods for population balance equations with coagulation, fragmentation and spatial inhomogeneity. J. Comput. Phys. **303**, 1–18 (2015)
42. Zhao, H., Zheng, C., Xu, M.: Multi-Monte Carlo approach for general dynamic equation considering simultaneous particle coagulation and breakage. Powder Technol. **154**(2–3), 164–178 (2005)
43. Kotalczyk, G., Devi, J., Kruis, F.E.: A time-driven constant-number Monte Carlo method for the GPU-simulation of particle breakage based on weighted simulation particles. Powder Technol. **317**, 417–429 (2017)
44. Devi, J., Kotalczyk, G., Kruis, F.E.: Accuracy control in Monte Carlo simulations of particle breakage. Int. J. Model. Ident. Control **31**(3), 278–291 (2019)
45. Muscato, O., Di Stefano, V., Wagner, W.: A variance-reduced electrothermal Monte Carlo method for semiconductor device simulation. Comput. Math Appl. **65**(3), 520–527 (2013)
46. Ziff, R.M., McGrady, E.D.: The kinetics of cluster fragmentation and depolymerisation. J. Phys. A: Math. Gen. **18**(15), 3027–3037 (1985)
47. Celnik, M., Patterson, R.I.A., Kraft, M., Wagner, W.: Coupling a stochastic soot population balance to gas-phase chemistry using operator splitting. Combust. Flame **148**(3), 158–176 (2007)
48. Liffman, K.: A direct simulation Monte-Carlo method for cluster coagulation. J. Comput. Phys. **100**(1), 116–127 (1992)
49. Zhao, H., Maisels, A., Matsoukas, T., Zheng, C.: Analysis of four Monte Carlo methods for the solution of population balances in dispersed systems. Powder Technol. **173**(1), 38–50 (2007)
50. Wei, J.: A parallel Monte Carlo method for population balance modeling of particulate processes using bookkeeping strategy. Physica A **402**, 186–197 (2014)
51. Kotalczyk, G., Kruis, F.E.: Fractional Monte Carlo time steps for the simulation of coagulation for parallelized flowsheet simulations. Chem. Eng. Res. Des. **136**, 71–82 (2018)
52. Gelbard, F., Tambour, Y., Seinfeld, J.H.: Sectional representations for simulating aerosol dynamics. J. Colloid Interface Sci. **76**(2), 541–556 (1980)
53. Landgrebe, J.D., Pratsinis, S.E.: A discrete-sectional model for particulate production by gas-phase chemical reaction and aerosol coagulation in the free-molecular regime. J. Colloid Interface Sci. **139**(1), 63–86 (1990)
54. Marshall, C.L., Rajniak, P., Matsoukas, T.: Multi-component population balance modeling of granulation with continuous addition of binder. Powder. Technol. **236**, 211–220 (2013)
55. Khalili, S., Lin, Y., Armaou, A., Matsoukas, T.: Constant number Monte Carlo simulation of population balances with multiple growth mechanisms. AIChE J. **56**(12), 3137–3145 (2010)

56. Smith, M., Matsoukas, T.: Constant-number Monte Carlo simulation of population balances. Chem. Eng. Sci. **53**(9), 1777–1786 (1998)
57. Kotalczyk, G., Lambach, K., Kruis, F.E.: Parallel GPU-based monte carlo techniques for the flow-sheet simulation of solid processes. In: 8th World Congress on Particle Technology (2018)−Applications of Solids Processing Unit Operations, pp. 64–71
58. Kumar, S., Ramkrishna, D.: On the solution of population balance equations by discretization –I. A fixed pivot technique. Chem. Eng. Sci. **51**(8), 1311–1332 (1996)